Available online at www.sciencedirect.com
SCIENCE DIRECT®
International Journal of Heat and Mass Transfer 48 (2005) 3423–3434
International Journal of HEAT and MASS TRANSFER
www.elsevier.com/locate/ijhmt

Modelling of radiation transfer in metallic powders at laser treatment

A.V. Gusarov [a,c,*], J.-P. Kruth [b]

[a] Russian Academy of Sciences, Baikov Institute of Metallurgy, Leninsky Prospect 49, 119991 Moscow, Russia
[b] Department of Mechanical Engineering, University of Leuven (K.U. Leuven), PMA, Celestijnenlaan 300B, 3001 Leuven, Belgium
[c] Graduate School of Engineering, Department of Aeronautics Astronautics, Kyoto University, Kyoto 606-8501, Japan

Received 12 December 2003; received in revised form 10 November 2004

Abstract

Absorptances and deposited energy profiles are calculated for thin layers of metallic powder placed on a reflective substrate at normal incidence of collimated radiation. Radiation transfer equation is analytically solved by the two-flux method. The effective optical parameters of the powder are estimated in geometrical optics approximation taking into account dependent scattering. The cases of specularly and diffusely reflecting particles are studied. Due to multiple reflections in an open pore system, laser radiation can penetrate in powder to considerable depths, much greater than the characteristic particle diameter. Total laser energy absorbed in a thin powder layer on a reflective substrate increases with its thickness but the deposited energy density decreases. Generally, the absorptance and the energy density for specular reflection are slightly greater than these values for diffuse reflection. The results obtained in the limit of deep powder bed essentially agree with known ray tracing simulations. The present model is in good agreement with experimentally observed correlation between effective absorptance of metallic powders and absorptance of corresponding dense metals.

Keywords: Powder bed; Radiation transfer equation; Dependent scattering; Effective absorptance; Deposited energy

1. Introduction

Consolidation of loose powder by local laser heating is becoming a promising manufacturing technique because of easy control over both powder deposition and laser radiation. One of the well-known examples is laser cladding [1]. Such rapid prototyping and manufacturing methods as selective laser sintering [2] and selective laser melting [3] are being developed. The essential operation is laser beam scanning over the surface of a thin powder layer previously deposited on a substrate. Powder binding mechanisms, such as melting and solid-state and liquid-phase sintering, strongly depend on temperature and so estimating local temperature fields is very important for process control.

The first problem arising when one attempts to calculate the temperature induced by a scanning laser beam is laser energy deposition. This includes not only an absorbed fraction of laser energy but also a depth

* Corresponding author. Address: Graduate School of Engineering, Department of Aeronautics Astronautics, Kyoto University, Kyoto 606-8501, Japan. Tel.: +81 75 753 4943; fax: +81 75 753 4942.
E-mail address: av.gusarov@relcom.ru (A.V. Gusarov).

0017-9310/$ - see front matter © 2005 Elsevier Ltd. All rights reserved.
doi:10.1016/j.ijheatmasstransfer.2005.01.044

Nomenclature

A	absorptance
a	eigenvalue factor
C_1, C_2	constants in general solution
c	fraction of collimated radiation scattered into the forward hemisphere
D	particle diameter
F	angular intensity of diffuse radiation
f	dimensionless angular intensity of diffuse radiation
G	collimated radiation intensity
g	dimensionless collimated radiation intensity
h	fraction of radiation uniformly distributed over a hemisphere that remains in the hemisphere after scattering
I	angular radiation intensity
L	layer thickness
n	number of particles per unit volume
P	scattering phase function
$\mathbf{Q}$	net radiative energy flux
q	dimensionless net radiative energy flux
R	particle radius
S	specific area of powder per unit pore volume
s	directional specific area per unit pore volume
U	specific surface area per unit mass
u	dimensionless deposited energy density
w	mass fraction
$\mathbf{x}$	radius vector
x, y, z	coordinates

Greek symbols

α	scattering angle
β	extinction coefficient
γ	scaling factor
δ	theoretical density
ϵ	porosity
θ	polar angle
κ	absorption coefficient
Λ	wavelength
λ	optical thickness
ξ	dimensionless coordinate
ρ	reflectance
σ	scattering coefficient
φ	azimuth angle
χ	angle of incidence
ψ	angle of reflection
$\mathbf{\Omega}$	unit vector of direction
ω	albedo

distribution of the absorbed energy because the incident radiation penetrates into the powder due to multiple reflections in an open pore system. The penetration is especially important for highly reflective metallic powders as indicated by ray tracing simulation [4]. The ray tracing technique [4,5] requires specifying the detailed powder structure by particles shape, dimension, and their coordinates that is a complicated problem itself and requires additional assumptions. To avoid such a problem in this work, powder is considered as a homogenous absorbing and scattering continuum with effective radiation transfer properties equivalent to those of a powder bed.

Radiation in the powder is characterized by the distribution of its angular intensity, $I(\mathbf{x}, \mathbf{\Omega})$, so that $\mathbf{\Omega} I(\mathbf{x}, \mathbf{\Omega})\,\mathrm{d}\mathbf{\Omega}$ is the energy flux density transferred by photons directed about the unit vector $\mathbf{\Omega}$ within solid angle $\mathrm{d}\mathbf{\Omega}$ at point $\mathbf{x}$. Effective value of the intensity is meant when considering a heterogeneous medium such as loose powder. That is, the local value is averaged over a volume much greater than a particle. The net radiative energy flux density is defined as an integral over all directions:

$$\mathbf{Q} = \int_{4\pi} \mathbf{\Omega} I \,\mathrm{d}\mathbf{\Omega}. \tag{1}$$

In absorbing and scattering medium the angular radiation intensity is governed by the radiation transfer equation (RTE) [6]:

$$\mathbf{\Omega} \nabla I = -(\sigma + \kappa) I + \frac{\sigma}{4\pi} \int_{4\pi} I(\mathbf{\Omega}')\, P(\mathbf{\Omega}' \to \mathbf{\Omega})\,\mathrm{d}\mathbf{\Omega}', \tag{2}$$

where σ and κ are the scattering and absorption coefficients, respectively, and $P(\mathbf{\Omega}' \to \mathbf{\Omega})$ the scattering phase function, which represents the probability that the radiation propagating in direction $\mathbf{\Omega}'$ is scattered to direction $\mathbf{\Omega}$. The phase function is normalised:

$$\frac{1}{4\pi} \int_{4\pi} P(\mathbf{\Omega}' \to \mathbf{\Omega})\,\mathrm{d}\mathbf{\Omega}' = 1. \tag{3}$$

Instead of the pair σ and κ one often use the extinction coefficient $\beta = \sigma + \kappa$ and albedo $\omega = \sigma/\beta$.

This article deals with the general problem of normal incidence of collimated radiation on a thin powder layer placed on a reflecting substrate. This configuration is typical for laser manufacturing [2]. Effective radiation transfer properties of metallic powders are theoretically estimated in Section 2. The RTE equation (2) is analytically solved by the two-flux method [7] in Sections 3 and 4. In Section 5, the obtained results on energy deposition profiles are compared with ray tracing simulation [4,8]

and the results on absorptance are compared with experiments [9].

2. Effective radiation-transfer properties of metallic powders

Light scattering by spherical particles is generally described by the Mie theory [10]. Currently, powders most widely used in laser manufacturing consist of particles with diameter D of several tens microns [2]. Scattering of laser radiation by such large particles often reduces to refraction and reflection in the geometrical optics approximation. Thus, in a cloud of opaque spheres of radius R considered as independent scattering centres, extinction coefficient β_i and albedo ω_i are [7]:

$$\beta_i = \pi R^2 n, \quad \omega_i = \rho, \tag{4}$$

where n is the number of particles per unit volume and ρ the hemispherical reflectance of the particle surface. It is noteworthy that the extinction coefficient is determined by geometrical parameters only and is independent of the material and wavelength. In contrast, the albedo, which is equal to reflectance, is independent of the geometry but includes the mentioned physical dependences. The specular and diffuse reflection laws give phase functions P_s and P_d, respectively [7]:

$$P_s = \rho'\left(\frac{\pi-\alpha}{2}\right)\Big/\rho, \tag{5}$$

$$P_d = \frac{8}{3\pi}(\sin\alpha - \alpha\cos\alpha), \tag{6}$$

where α is the scattering angle and $\rho'(\chi)$ the directional specular reflectance depending generally on incidence angle $\chi = (\pi - \alpha)/2$. Diffuse reflection is independent of incidence angle. Eq. (5) gives isotropic scattering in case of directional reflectance independent of incidence angle.

It is known [10] that taking into account small-angle diffraction effects at particle diameter D much greater than wavelength Λ, leads to doubling extinction coefficient (4) while a strong forward-directed diffraction term arises in phase function (5) and (6). However, the significant difference is only apparent. The issue is whether to consider the small-angle diffraction as extinction or to neglect it. In practice, the geometrical optics formulas (4)–(6) can be applied [7] when

$$\pi D/\Lambda \geqslant 5. \tag{7}$$

The simple theory described above is valid only if the particles are spherical and each particle scatters radiation independently of its neighbours.

2.1. Statistical scattering model

Consider a powder bed (PB) composed of opaque particles of arbitrary shapes and dimensions with the only restriction that the curvature radius of the surface is greater than the wavelength. According to Eq. (7), this allows applying geometrical optics. The structure of PB is characterized by such parameters as porosity ε (volume fraction of pores) and specific surface area (total surface area of particles) per unit mass U. In the studied powder beds of opaque particles, radiation can not penetrate into particles and is concentrated in pores. Therefore, specific surface area per unit pore volume $S = \delta(1-\varepsilon)U\varepsilon$ is introduced with δ being the density of the solid phase (theoretical density). Distribution of specific surface S over directions is specified by directional volumetric specific surface area of the powder $s(\mathbf{\Omega})$, so that $s(\mathbf{\Omega})\,\mathrm{d}\mathbf{\Omega}$ is the area of the particles' surface with the external normal about unit vector $\mathbf{\Omega}$ within solid angle $\mathrm{d}\mathbf{\Omega}$ per unit pore volume of PB.

Consideration of radiation transfer through a thin powder layer gives its effective parameters. Thus, the extinction and scattering coefficients are obtained by averaging over directions of the surface normal within a hemisphere where incidence angle χ is less than $\pi/2$ (see Fig. 1):

$$\beta = \int_{2\pi} \cos\chi s(\mathbf{\Omega})\,\mathrm{d}\mathbf{\Omega}, \tag{8}$$

$$\sigma = \int_{2\pi} \rho'(\chi)\cos\chi\, s(\mathbf{\Omega})\,\mathrm{d}\mathbf{\Omega}, \tag{9}$$

where $\mathrm{d}\mathbf{\Omega} = \mathrm{d}\varphi\,\mathrm{d}\cos\chi$ and φ is the azimuth angle.

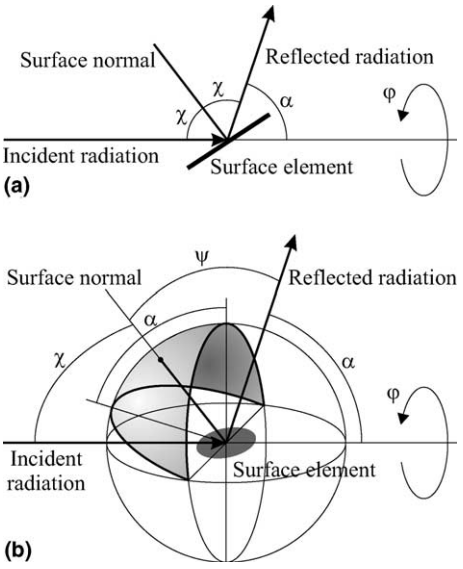

Fig. 1. Schemes of scattering: (a), specular reflection, fixed surface normal orientation for a given scattering direction; (b) diffuse reflection, the radiation scattered into a specified direction arises from surface elements oriented within the shadowed region of the unit sphere. Angles: χ, incidence; ψ, reflection; α, scattering; φ, azimuth.

In case of specular reflection, scattered radiation intensity at scattering angle α and azimuth angle φ is proportional to surface area at the direction satisfying the specular reflection condition with incidence angle $\chi = (\pi - \alpha)/2$ and azimuth angle φ as shown in Fig. 1(a): $\mathrm{d}I(\alpha,\varphi) \sim \rho'(\chi)\cos\chi s(\chi,\varphi)\,\mathrm{d}\varphi\,\mathrm{d}\cos\chi \sim \rho'(\chi)s(\chi,\varphi)\,\mathrm{d}\varphi\,\mathrm{d}\cos\alpha$. Taking into account normalising condition (3), the scattering phase function at specular reflection is expressed as

$$P_s(\alpha,\varphi) = \frac{\pi\rho'(\chi)s(\chi,\varphi)}{\int_0^1 \rho'(\chi)\cos\chi\,\mathrm{d}\cos\chi\int_0^{2\pi} s(\chi,\varphi)\,\mathrm{d}\varphi}. \tag{10}$$

Diffuse reflection gives the scattered intensity proportional to the integral over surface elements with normals oriented within the shadowed region of the unit sphere as shown in Fig. 1(b):

$$P_d(\alpha,\varphi) \sim \int_{\pi/2}^{\pi/2+\alpha}\mathrm{d}\alpha'\int_{-1}^{1}\rho'(\chi) \times \cos\chi\cos\psi\; s(\varphi',\alpha')\,\mathrm{d}\cos\varphi'. \tag{11}$$

where χ is the incidence and ψ the reflection angles. Integration is performed in Eq. (11) in a spherical coordinate system with the polar angle φ' and the azimuth angle α' and the axis $\varphi' = 0$ corresponding to the scattering polar angle $\alpha = \pi/2$ and the scattering azimuth angle $\varphi - \pi/2$. The incidence and reflection angles are obtained from the following equations:

$$\cos\chi = \sin\varphi'\cos\alpha', \quad \cos\psi = \sin\varphi'\cos(\alpha' - \alpha). \tag{12}$$

If there is no preferential orientation of particles, surface area distribution is isotropic:

$$s(\mathbf{\Omega})\,\mathrm{d}\mathbf{\Omega} = S\,\mathrm{d}\mathbf{\Omega}/(4\pi), \tag{13}$$

where S is the specific surface area of the powder per unit pore volume. Then Eqs. (8) and (9) give the following expressions for extinction β and scattering σ coefficients and albedo $\omega = \sigma/\beta$:

$$\beta = S/4, \quad \sigma = \rho\quad S/4, \quad \omega = \rho, \tag{14}$$

where the definition of the hemispherical reflectance [7],

$$\rho = \frac{1}{\pi}\int_{2\pi}\rho'(\chi)\cos\chi\,\mathrm{d}\mathbf{\Omega}, \tag{15}$$

is taken into account. One can see from Eq. (14) that only a quarter of the powder surface is effective in scattering. A factor of 1/2 arises because, in average, only a half of particle surface is exposed to the radiation of a specified direction. Another factor of 1/2 originates from integrating of cos χ over a hemisphere. Physically, this means that not the surface but its cross-section visible in the direction of irradiation is important. In the isotropic case, integration in Eqs. (10) and (11) gives the same result as for spherical particles. The phase function is given by Eq. (5) for specular reflection and by Eq. (6) for diffuse reflection.

2.2. Powder mixtures

The above model can be extended to powder mixtures. Let the mixture of porosity ε be composed of K components with mass fractions w_k, theoretical densities δ_k, and specific surface areas per unit mass U_k, $k = 1,\ldots,K$. Total specific area is

$$U = \sum U_k w_k. \tag{16}$$

The scattering properties of each component are characterised by albedo ω_k and phase function P_k. Extinction coefficient β, albedo ω, and phase function P of the mixture are then calculated as

$$\beta = \frac{1-\varepsilon}{4\varepsilon}\frac{U}{\sum w_k/\delta_k}, \tag{17}$$

$$\omega = \frac{\sum \omega_k U_k w_k}{U}, \tag{18}$$

$$P = \frac{\sum \omega_k P_k U_k w_k}{\omega U}. \tag{19}$$

Eqs. (17)–(19) estimate radiation transfer properties of a powder mixture with known properties of its components.

2.3. Dependent scattering

In dense PBs where particles touch each other, radiation transfer can not be treated as scattering by separate particles [11]. This effect is referred to as dependent scattering and has been studied in a number of experimental [12–14] and theoretical [5,11,15,16] works.

For a PB of equal spherical particles with radius R, specific area per unit pore volume is

$$S = \frac{4\pi R^2 n}{\varepsilon}, \tag{20}$$

where n is the number of particles per unit volume of PB and $\varepsilon = 1 - 4\pi R^3 n/3$ is the porosity (total volume of pores per unit volume of PB). This gives the following relation between independent scattering by opaque spheres (4) and the statistical model (14):

$$\beta = \gamma\beta_i, \quad \sigma = \gamma\sigma_i, \quad \omega = \omega_i, \tag{21}$$

where a scaling factor is introduced,

$$\gamma = 1/\varepsilon. \tag{22}$$

Eqs. (21) and (22) reduce to independent scattering (4) at high porosities, $\varepsilon \to 1$, when scaling factor γ tends to unity. A considerable difference arises in dense PBs due to dependent scattering, which is actually a mutual influence of scattering particles. Dependent scattering has no effect on the phase function according to the present model. A simple interpretation of Eq. (22) is that

radiation does not penetrate into opaque particles and so the apparent concentration of scattering centres should be calculated not per unit volume of PB but per unit volume of pores.

Singh and Kaviany [5] obtained similar scaling relations (21) describing their ray tracing simulation results in a wide range of porosity $0.3 < \varepsilon < 1$. They also concluded that dependent scattering does not influence the phase function and that the scaling factor is a function of porosity. The analytical approximation of the function $\gamma(\varepsilon)$ derived in [5] differs from Eq. (22) but actually gives very close values in the considered porosity range as shown in Fig. 2.

Kamiuto [15] attempted to estimate the dependent scattering effects theoretically and obtained different scaling relations:

$$\beta = \gamma\beta_i, \quad (1-\omega) = (1-\omega_i)/\gamma. \tag{23}$$

However, they are equivalent to Eq. (21) in case of highly reflective metallic powders with albedo $\omega \to 1$. Function $\gamma(\varepsilon)$ reported in [15] is plotted in Fig. 2. It agrees with the present model at high porosities $\varepsilon > 0.7$ and considerably differs for more dense powders.

Tancrez and Taine [16] studied two models for porous structures: Dispersed radius Overlapping Opaque Spheres (DOOS) in a transparent matrix and Dispersed radius Overlapping Transparent Spheres (DOTS) in an opaque matrix. They showed that Eq. (14) are rigorous for optically thin layers of the both structures and for DOOS of arbitrary thickness. On the other hand, Monte Carlo investigation of the DOTS model [16] gives stronger extinction in thick layers than predicted by Eq. (14). This can be described by Eq. (21) where the scaling factor is higher than specified by Eq. (22). The difference in scaling factor increases with the density and reaches the factor of 1.5 at the porosity $\varepsilon = 0.4$, which is typical for powders employed in rapid manufacturing [2].

Thus, the DOTS model is an example where the simple statistical scattering model described in Section 2.1 and Section 2.2, is not accurate. This discrepancy may originate from the general limitation of description of heterogeneous medium by effective properties. In particular, the extinction length is comparable with particles' size in dense PBs. On the other hand, the DOTS structure is rather complicate that can correspond to powders with highly irregular particles only. Powders with about spherical particles are better described by DOOS structure where Eqs. (14), (21) and (22) are rigorous [16]. The same rigorous result can be obtained for non-overlapping opaque spheres in a transparent matrix considering the chord-length distribution estimated in [17].

Monte Carlo identification [16] indicates that, in general, the phase function of a dense PB differs from that given by the independent theory, Eqs. (5) and (6). However, in case of DOOS model with the specular reflection law, the phase function becomes about isotropic at high reflectances [16]. This justifies applying Eq. (5) for metallic powders.

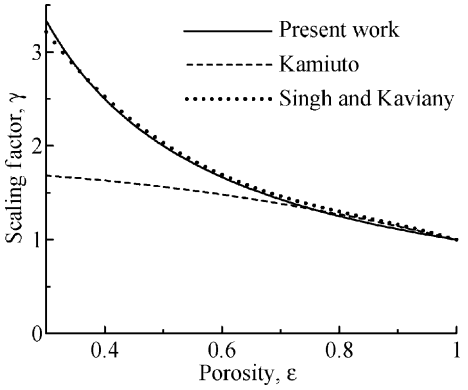

Fig. 2. Scaling factor to take into account dependent scattering: full line, present model, Eq. (22); dashed line, theoretical estimations by Kamiuto [15]; dotted line, fit to ray tracing simulation by Singh and Kaviany [5].

3. Radiation transfer model

Fig. 3(a) shows the general configuration of PB used in modelling. A powder layer of thickness L is placed on a specularly reflecting substrate. Thus, one can simulate thin powder layers on metallic substrates as well as deep powder beds at $L \to \infty$ where the influence of the substrate is negligible. The Cartesian frame is introduced, so that axis (OZ) is directed along the inner normal to the powder bed surface and axes (OX) and (OY) lay on the surface. Thus, z-coordinate is in fact the depth. Normally incident laser radiation is assumed to be distributed over a spot at the powder bed surface with a size much greater than the radiation penetration depth. Therefore, radiation intensity distribution in lateral

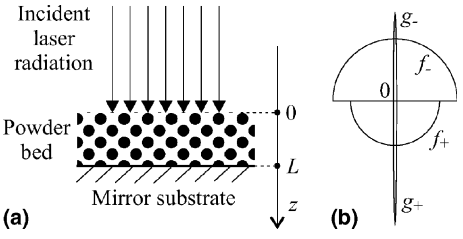

Fig. 3. Scheme of the considered configuration of powder bed (a) and typical angular diagram of radiation intensity in the two-flux approximation (b). Radiation components: g_+, forward collimated; g_-, backward collimated; f_+, forward diffuse; f_-, backward diffuse.

directions follows the distribution of incident laser energy flux density over the surface $G_0(x,y)$ and the considered problem is one-dimensional. Lateral coordinates x and y are omitted below to simplify notation, although they are actually taken into account through function $G_0(x,y)$.

In one-dimensional case, the general RTE (2) reduces to:

$$\cos\theta\frac{\partial I}{\partial z}=\beta\left\{\frac{\omega}{2}\int_{-1}^{1}I(\theta')P_r(\theta',\theta)\,\mathrm{d}\cos\theta'-I(\theta)\right\},\qquad(24)$$

where angular radiation intensity $I(z,\theta)$ and reduced phase function $P_r(\theta',\theta)$ are independent of azimuth angle. In isotropic media, phase function $P(\alpha)$ depends on scattering angle α only, like in Eqs. (5) and (6), and the scattering angle, in turn, depends on polar angles of incident radiation, θ', and scattered radiation,θ, and on the difference of azimuth angles φ': $\cos\alpha=\cos\theta\cos\theta'+\sin\theta\sin\theta'\cos\varphi'$. This allows defining the reduced phase function as

$$P_r(\theta',\theta)=\frac{1}{2\pi}\int_0^{2\pi}P(\alpha)\,\mathrm{d}\varphi',\qquad(25)$$

Eq. (24) is solved in segment $z=0,\ldots,L$. Incident laser radiation is assumed to be directed along the normal to the powder bed surface that gives the boundary condition of normal incidence at $z=0$:

$$I(0,\theta)=\frac{G_0}{2\pi}\delta(\cos\theta-1),\quad\text{at }\theta<\frac{\pi}{2},\qquad(26)$$

where $\delta(x)$ denotes the Dirac delta-function. At plane $z=L$ the boundary condition of complete specular reflection is used:

$$I(L,\theta)=I(L,\pi-\theta).\qquad(27)$$

Angular radiation intensity can be expressed as the sum

$$I(z,\theta)=\frac{G_+(z)}{2\pi}\delta(\cos\theta-1)+\frac{G_-(z)}{2\pi}\delta(\cos\theta+1)+F(z,\theta),\qquad(28)$$

of collimated direct laser radiation and laser radiation reflected from the substrate with energy flux densities of G_+ and G_-, respectively, and diffuse radiation F. The diffuse term arises when the direct and back reflected laser radiation are scattered. Integrating Eqs. (24), (26) and (27) over $\cos\theta$ in small vicinities of forward, $\theta=0$, and backward, $\theta=\pi$, directions gives the following boundary problem to obtain the direct and back-reflected collimated radiation:

$$\frac{\mathrm{d}G_+}{\mathrm{d}z}=-\beta G_+,\quad\frac{\mathrm{d}G_-}{\mathrm{d}z}=\beta G_-,\qquad(29)$$

$$G_+(0)=G_0,\quad G_+(L)=G_-(L).\qquad(30)$$

The solution of this problem is:

$$G_+=G_0\exp(-\xi),\quad G_-=G_0\exp(\xi-2\lambda),\qquad(31)$$

where $\xi=\beta z$ is the dimensionless coordinate and $\lambda=\beta L$ the optical thickness. One can obtain from Eqs. (24), (26) and (27) the following boundary problem for diffuse radiation:

$$\cos\theta\frac{\partial f}{\partial\xi}=\frac{\omega}{2}P_r(0,\theta)g_+ +\frac{\omega}{2}P_r(\pi,\theta)g_- +\frac{\omega}{2}\int_{-1}^{1}f(\theta')P_r(\theta',\theta)\,\mathrm{d}\cos\theta'-f,\qquad(32)$$

$$f(0,\theta)=0,\quad\text{at }\theta<\pi/2,\qquad(33)$$

$$f(\lambda,\theta)=f(\lambda,\pi-\theta),\qquad(34)$$

where the following dimensionless parameters are used: $f=F/G_0$ is the diffuse radiation intensity and $g_+=G_+/(2\pi G_0)$ and $g_-=G_-/(2\pi G_0)$ the forward and backward collimated radiation intensities, respectively. The first term in the right-hand side of Eq. (32) is the diffuse radiation source due to scattering of direct collimated radiation. The second term is due to scattering of back-reflected collimated radiation. The third term is the source due to scattering of the diffuse radiation from other directions, and the forth term is the sink caused by scattering and absorption.

Eqs. (32)–(34) are solved by the two-flux method [7] as follows. The diffuse radiation intensity is approximated as

$$f(\xi,\theta)=f_+(\xi)\Phi_+(\theta)+f_-(\xi)\Phi_-(\theta),\qquad(35)$$

where function $\Phi_+(\theta)$ is equal to unity in the forward hemisphere, $\theta<\pi/2$, and zero otherwise. Function $\Phi_-(\theta)$, on the contrary, is equal to unity in the backward hemisphere, $\theta>\pi/2$, and zero in the forward one. As shown in Fig. 3(b), total radiation intensity is approximated by a superposition of two collimated and two diffuse components.

Integrating equation (32) multiplied by $\Phi_+(\theta)$ or $\Phi_-(\theta)$ over $\cos\theta$ from -1 to 1 gives two moment equations:

$$\frac{1}{2}\frac{\mathrm{d}f_+}{\mathrm{d}\xi}=-(1-h\omega)f_+ +(1-h)\omega f_- +\omega[cg_+ +(1-c)g_-],\qquad(36)$$

$$-\frac{1}{2}\frac{\mathrm{d}f_-}{\mathrm{d}\xi}=-(1-h\omega)f_- +(1-h)\omega f_+ +\omega[(1-c)g_+ +cg_-],\qquad(37)$$

where

$$h=\frac{1}{2}\int_0^1\mathrm{d}\cos\theta\int_0^1 P_r(\theta',\theta)\,\mathrm{d}\cos\theta',\qquad(38)$$

is the fraction of radiation uniformly distributed over a hemisphere that remains in the hemisphere after scattering and

Table 1
Coefficients of the two-flux equations for different scattering models

Coefficients	h	c
Specular reflection	$\frac{1}{2}$	$\frac{1}{2}$
Diffuse reflection	$\frac{1}{3}$	$\frac{1}{6}$

$$c = \frac{1}{2}\int_0^1 P_r(0,\theta)\,\mathrm{d}\cos\theta, \tag{39}$$

is the fraction of collimated radiation scattered into the forward hemisphere. Coefficients h and c corresponding to the two particular cases of specular and diffuse reflection specified by Eqs. (5) and (6) are listed in Table 1. Specular reflection is assumed to be independent of incidence angle.

Eqs. (36) and (37) are to be solved with the following boundary conditions:

$$f_+(0) = 0, \quad f_+(\lambda) = f_-(\lambda). \tag{40}$$

4. Results

The general solution of Eqs. (36) and (37) can be expressed as

$$\begin{aligned} f_+ = {} & C_1\exp(-2a\xi) + C_2\exp(2a\xi) \\ & - \frac{1}{\pi}\frac{\omega}{1-4a^2}\{[3c + 2\omega(1-h-c)]\exp(-\xi) \\ & + [1 - c - 2\omega(h-c)]\exp(\xi - 2\lambda)\}, \end{aligned} \tag{41}$$

$$\begin{aligned} f_- = {} & \frac{1}{(1-h)\omega}[C_1(1 - h\omega - a)\exp(-2a\xi) \\ & + C_2(1 - h\omega + a)\exp(2a\xi)] \\ & - \frac{1}{\pi}\frac{\omega}{1-4a^2}\{[1 - c - 2\omega(h-c)]\exp(-\xi) \\ & + [3c + 2\omega(1-h-c)]\exp(\xi - 2\lambda)\}, \end{aligned} \tag{42}$$

where a is the eigenvalue factor, $a^2 = 1 - 2h\omega - \omega^2(1-2h)$. Constants C_1 and C_2 are found from boundary conditions (40):

$$\begin{aligned} C_1 = {} & \frac{1}{\pi}\frac{\omega(1-\omega+a)}{1-4a^2} \\ & \times \frac{3c + 2\omega(1-h-c) + [1-c-2\omega(h-c)]\exp(-2\lambda)}{1-\omega+a-(1-\omega-a)\exp(-4a\lambda)}, \end{aligned} \tag{43}$$

$$C_2 = -C_1\frac{1-\omega-a}{1-\omega+a}\exp(-4a\lambda). \tag{44}$$

Table 2
Dimensionless optical characteristics of powder

Conditions	Name	Definition
Thin powder layer on a reflective substrate	Energy flux	$q^\lambda = Q_z/G_0$
	Deposited energy	$u^\lambda = -\nabla\mathbf{Q}/(\beta G_0) = -\mathrm{d}q^\lambda/\mathrm{d}\xi$
	Absorptance	$A_e^\lambda = q^\lambda(0)$
Deep powder bed	Energy flux	$q = \lim_{\lambda\to\infty} q^\lambda$
	Deposited energy	$u = -\nabla\mathbf{Q}/(\beta\ G_0) = -\mathrm{d}q/\mathrm{d}\xi$
	Absorptance	$A_e = q(0)$

Dimensionless net energy flux density in z-direction q^λ is obtained from Eq. (1):

$$\begin{aligned} q^\lambda = {} & Q_z/G_0 = \pi(f_+ - f_-) + 2\pi(g_+ - g_-) \\ = {} & -\frac{(1-\omega)^2 - a^2}{(1-h)(1-4a^2)} \\ & \times \frac{3c + 2\omega(1-h-c) + [1-c-2\omega(h-c)]\exp(-2\lambda)}{(1-\omega+a)\exp(2a\lambda) - (1-\omega-a)\exp(-2a\lambda)} \\ & \times \{\exp[2a(\lambda-\xi)] - \exp[2a(\xi-\lambda)]\} \\ & - \frac{(1-\omega)[1-4\omega(h-c)] + 2a^2}{1-4a^2}[\exp(-\xi) \\ & - \exp(\xi - 2\lambda)], \end{aligned} \tag{45}$$

When $\lambda \to \infty$, Eq. (45) gives energy flux density in a deep powder bed:

$$\begin{aligned} q = \lim_{\lambda\to\infty} q^\lambda = {} & -\frac{(1-\omega-a)[3c + 2\omega(1-h-c)]}{(1-h)(1-4a^2)\exp(2a\xi)} \\ & - \frac{(1-\omega)[1-4\omega(h-c)] + 2a^2}{(1-4a^2)\exp(\xi)} \end{aligned} \tag{46}$$

The definitions of powder optical characteristics used below are summarized in Table 2. Two of them are specified by Eqs. (45) and (46) and the others can be derived from these equations. A simple expression is obtained for absorptance of a deep powder bed:

$$A_e = \frac{(1-h-c)(1-\omega) + [2(1-h)+c]a}{(1-h)(1+2a)}, \tag{47}$$

which reduces to

$$A_e^s = \frac{3a}{1+2a}, \quad a = (1-\omega)^{1/2}, \tag{48}$$

in the case of specular reflection, and to

$$A_e^d = \frac{3}{4}\frac{1-\omega+3a}{1+2a}, \quad a = \left[1 - \frac{2}{3}\omega - \frac{1}{3}\omega^2\right]^{1/2}, \tag{49}$$

in the case of diffuse reflection.

5. Discussion

The statistical scattering model described in Section 2 is applicable to particles of arbitrary shape. According to this model, radiative properties (extinction and scattering coefficients and scattering phase function) in packed beds of non-spherical particles without preferential orientation (statistically isotropic) are the same as in packed beds of spherical particles with the same porosity and specific surface. This result is similar to that well-known from independent scattering theory [10]: randomly oriented irregular convex particles scatter like spheres. One can take into account preferential orientation of non-spherical particles through distribution of specific surface over orientation $s(\mathbf{\Omega})$ in Eqs. (8)–(11).

All calculations are made for statistically isotropic powder beds without regard to the shape of particles. However, this model is validated by comparison with ray tracing [4,8] only for spherical particles. Validation of the statistical scattering model for non-spherical particles requires further ray tracing simulation or experimental measurements with characterization of particles' shape.

Fig. 4 shows typical examples of depth profiles of radiative energy flux density $\mathbf{Q}$ and deposited energy density $-\nabla\mathbf{Q}$ in iron powder calculated according to Eqs. (45) and (46). Definitions of the corresponding dimensionless parameters are presented in Table 2. Two phase functions given by isotropic specular (5) and diffuse (6) reflection models are used. Two laser wavelengths of 1.06 and 10.6 μm are examined that correspond to Nd:YAG and CO_2 lasers, respectively. Albedos ω are estimated to be equal to reflectances of dense material ρ according to Eq. (14). The reflectance strongly depends on wavelength: Fe surface is considerably more reflective at 10.6 μm than at 1.06 μm. The numerical values of reflectance used in the calculations are taken from Ref. [4] and listed in Table 3.

Table 3
Parameters of Fe–Cu and WC–Co powder mixtures accepted in ray tracing simulation [4,8]

Parameter	Fe	Cu	WC	Co
Porosity of the mixture		0.75		0.75
Weight fraction	0.7	0.3	0.91	0.09
Theoretical density (g/cm^3)	7.87	8.96	15.7	8.90
Particle diameter (μm)	50	30	50	20
Reflectance at 1.06 μm	0.7	0.9	0.45	0.69
Reflectance at 10.6 μm	0.965	0.985	–	–

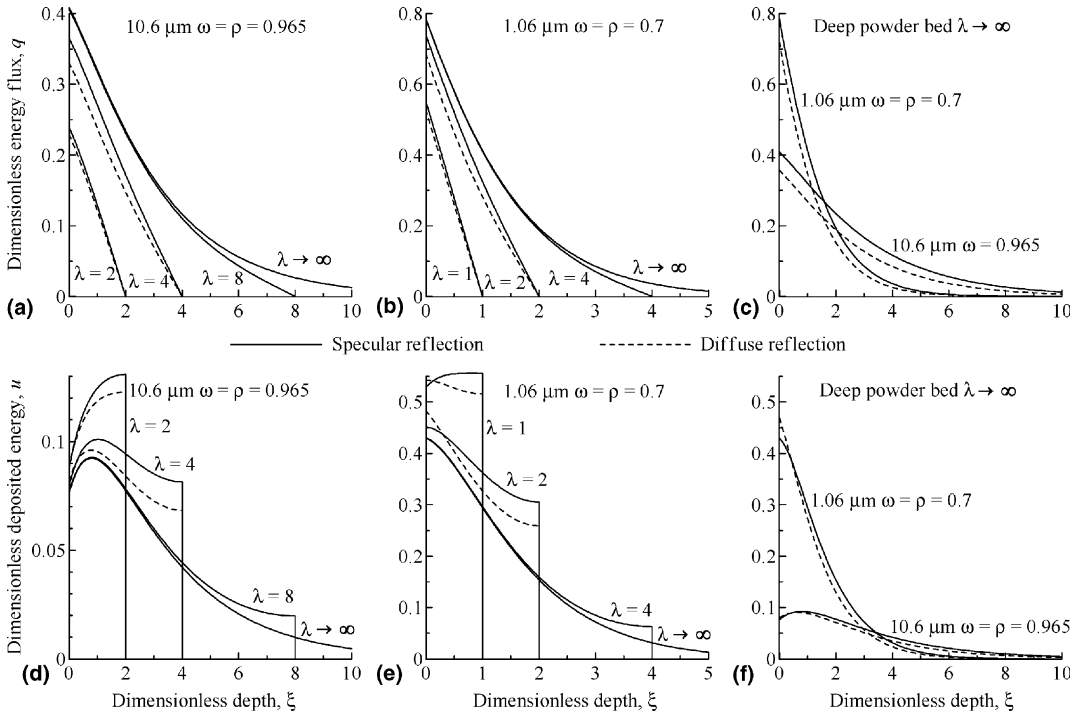

Fig. 4. Penetration of laser radiation into an iron powder bed: (a)–(c), radiative energy flux; (d)–(f), deposited energy density; (a), (b), (d), (e), thin powder layer on a completely reflecting substrate; (e), (f), deep powder bed. Dimensionless characteristics are defined in Table 2. The following parameters are marked in the graphs: laser wavelength, albedo ω equal to reflectance ρ of dense material, and optical thickness $\lambda = \beta L$. Full and broken lines represent the specular and diffuse reflection models, respectively.

Net radiative energy flux in a thin powder layer on a completely reflecting substrate q^{λ} monotonously decreases with depth (see Fig. 4(a) and (b)) and vanishes at the substrate where reflected radiation compensates the incident one. The flux at a given depth increases with the layer thickness because the back-reflected radiation, which reduces the net energy flux in the forward direction, is more pronounced for thinner layers. The depth of laser energy penetration into a deep powder bed increases with reflectance of dense material as shown in Fig. 4(c). In the case of CO_2 laser where the reflectance of iron is as high as 0.965, laser radiation is still significant at the dimensionless depth of ≈10.

Energy density deposited into a deep powder bed either monotonously decreases with depth at low reflectance (see 1.06 μm curves in Fig. 4(f)) or reaches a maximum in the bulk at high reflectance (see 10.6 μm curves in Fig. 4(f)). Deposited energy distribution in a thin layer can be monotonous or have a local maximum depending on the layer thickness (see Fig. 4(d)–(e)). The layer thickness impact on the deposited energy is opposite to the impact on the energy flux: the deposited energy density increases with decreasing the thickness. This behaviour is explained by substrate influence: the substrate reflects radiation and makes it pass through the powder once more in the backward direction. The increase of the deposited energy density in thin powder layers on reflective substrates is of particular importance for laser treatment of powders.

As follows from Fig. 4, the difference in both radiation flux and deposited energy between the specular (full lines) and diffuse (broken lines) reflection models is surprisingly low. Radiation flux at diffuse reflection is always less than that at specular reflection (see Fig. 4(a)–(c)). This can be explained by preferential backward scattering in the diffuse reflection model according to Eq. (6). This is why less radiation enters the powder at diffuse reflection. The dependence of deposited energy on reflection law is more complicated (see Fig. 4(d)–(f)) but one can conclude that, in average, the deposited energy density is less at diffuse reflection.

Laser radiation transfer in a deep powder bed has been already studied by ray tracing Monte Carlo simulation [4,8]. Iron–copper (Fe–Cu) [4] and tungsten carbide–cobalt (WC–Co) [8] powder mixtures have been studied. All the powder components (Fe, Cu, WC, and Co) were accepted to consist of spherical monodispersed specularly reflecting particles. The parameters taken for these simulations are listed in Table 3. Applying Eqs. (17) and (18) one can obtain the optical properties of the mixtures listed in Table 4. These parameters are used to obtain radiation flux and deposited energy profiles according to the present RTE model with the isotropic phase function of specular reflection (5). Fig. 5 compares RTE solutions (full lines) with ray tracing simulation (broken lines). The present calculations based on RTE agree in general with the ray tracing [4,8].

Table 4
Estimated optical parameters of the powder mixtures

Parameter	WC–Co	Fe–Cu	Fe–Cu
	1.06 μm	1.06 μm	10.6 μm
Extinction coefficient, β (mm^{-1})	12.23	11.82	11.82
Albedo, ω	0.52	0.78	0.973

The extinction length, $1/\beta$, for the both powder mixtures is less than 0.1 mm (see values of β in Table 4). However, radiation can penetrate into the powder beds (PB) substantially deeper, as shown in Fig. 5. For instance, radiation flux in the Fe–Cu mixture at 10.6 μm is still considerable at the depth of 0.7 mm (see Fig. 5(c)). Direct laser radiation attenuates proportionally to $\exp(-\beta z)$ (see Eq. (31)) and is negligible at such distance. Only diffuse radiation is responsible for the observed deep penetration that is due to multiple reflections of the incident radiation in the open pore system. The importance of the diffuse radiation increases with albedo ω, which can be considered as the average reflectance of particles in the mixture (see Eqs. (14) and (18)). This tendency is clear from Fig. 5.

The only significant difference between the RTE and the ray tracing results is in a thin layer adjacent to the PB surface where RTE technique considerably overestimates the deposited energy relative to ray tracing (see Fig. 5(d)–(f)). Note that the difference occurs within a particle diameter from the surface. The origin of the discrepancy is that the structure of PB near the surface changes. In particular, the porosity, ε, gradually grows to unity within about one surface monolayer. This effect is not taken into account by the present RTE model where a stepwise change of the porosity is implicitly assumed at the surface of PB.

The effective absorptance of a powder layer on a completely reflecting substrate, A_e^{λ} (defined in Table 2), increases with layer thickness (see Fig. 6) and reaches a plateau for thicker layers that corresponds to a deep powder bed. The higher is reflectance of dense material, the slower effective absorptance approaches the plateau. The effective absorptance value at the plateau decreases with the dense material reflectance. Absorptance for the specular reflection model (full lines in Fig. 6) is slightly higher than for the diffuse reflection model (broken lines). The difference in absorptance corresponds to the difference in radiation flux shown in Fig. 4(a)–(c). The absorptance at diffuse reflection is lower because of preferential backward scattering according to Eq. (6). Summarising the behaviour of thin powder layers on reflecting substrates, one can say that the total laser energy absorbed in the layer increases with its thickness but the energy density decreases.

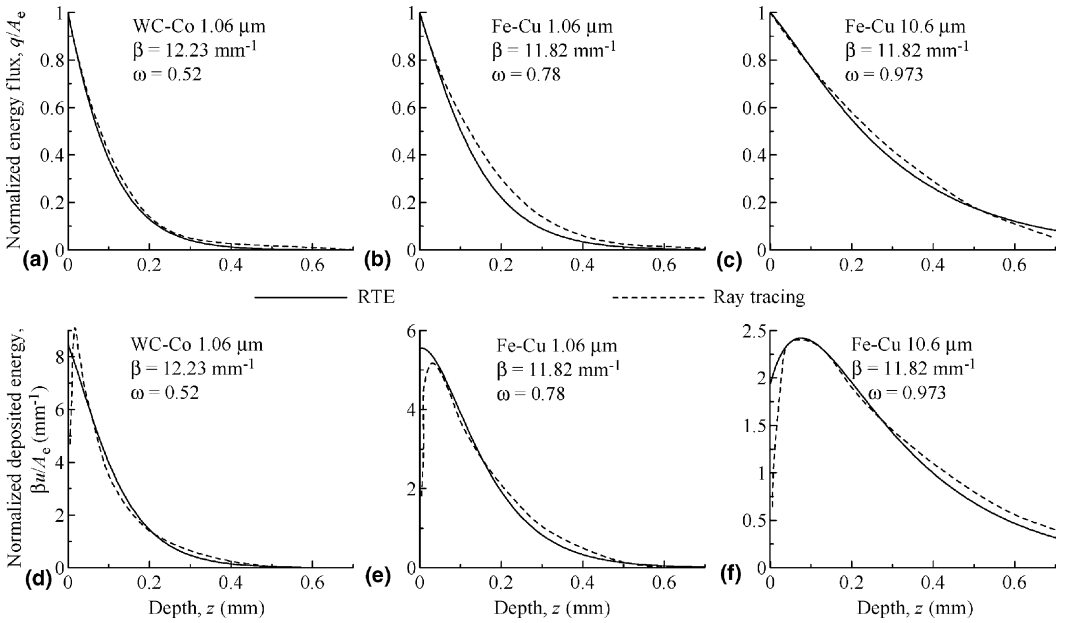

Fig. 5. Comparison of the present calculations based on RTE (full lines) with ray tracing simulation (broken lines) for the WC–Co [8] ((a), (d)) and Fe–Cu [4] ((b)–(c), ((e)–(f)) powder mixtures at the wavelengths of 1.06 μm and 10.6 μm: (a)–(c), energy flux; (d)–(f), deposited energy. Dimensionless values q and u are defined in Table 2.

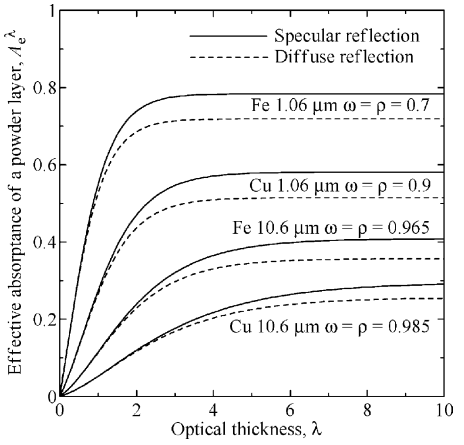

Fig. 6. Effective absorptance of a powder layer on a completely reflecting substrate versus layer thickness: full lines, isotropic specular reflection model (5); broken lines, diffuse reflection model (6). Powder material, laser wavelength, and reflectance of dense material ρ taken for the calculations are marked near the corresponding curves.

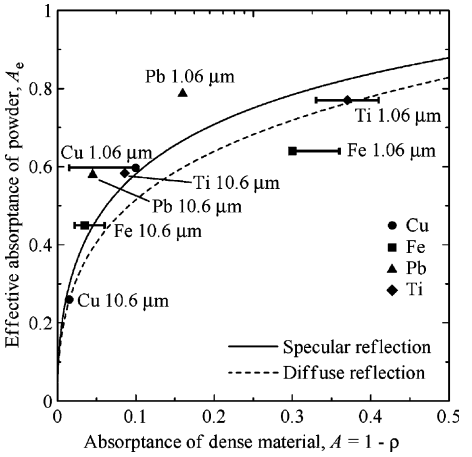

Fig. 7. Effective absorptance A_e of a deep powder bed versus absorptance A of dense material: full line, isotropic specular reflection model (5); broken line, diffuse reflection model (6); points, experimental data [9,18–22]. Powder material and laser wavelength are marked near the experimental points.

Fig. 7 shows the effective absorptance of a deep powder bed, A_e versus the absorptance of dense material, $A = 1 - \rho$, for the specular (full line) and diffuse (broken line) reflection laws calculated according to Eqs. (47)–(49). There is no much difference between the two reflection laws. Both curves pass the points $\{A = 0;\ A_e = 0\}$ and $\{A = 1;\ A_e = 1\}$ and are monotonous in the interval $0 < A < 1$. Effective absorptance of powder A_e can be considerably higher than the absorptance of the corresponding dense material A in the interval $0 < A < 1$. This behaviour seems to be reasonable because only a part of radiation is reflected by particles at the surface of PB.

The rest enters the pores and is absorbed inside PB. The ray tracing method [4] gives qualitatively the same functions of A_e versus A.

The calculated curves are compared with experimental measurements for metallic powders (points in Fig. 7). The powder effective absorptances are taken from [9] and the corresponding dense material absorptances are taken from [18–22]. Note that different methods of measurement and sample preparation give rather different values of absorptance of dense material [18–22]. The points generally correspond to direct reflectance measurements of a smooth surface of a polycrystalline sample [18]. Horizontal bars indicate uncertainty in the absorptance of dense material. The experimental data demonstrate a strong correlation between the absorptance of powder and that of dense material that approximately agrees with the calculated curves. The experimental error is about the difference between the specular (full line) and diffuse (broken line) scattering models. Therefore, one can not conclude which of the two models describes the experiments better. More careful characterization of powder structure and the state of the particles' surface is necessary to study the influence of these factors on the optical properties.

In this work only perfectly reflecting substrates are studied. Ray tracing simulation [4,5] and two-flux analytical solutions [5] have been reported for layers with transmission boundary conditions at the back surface that are equivalent to completely absorbing substrate. One can qualitatively estimate the influence of non-perfectly reflecting substrate by comparison of these limiting cases. Absorption by the substrate should reduce radiation flux propagating in the back direction. This increases absorptance of the system powder layer-substrate but decreases energy deposited in the powder.

6. Conclusion

Laser radiation transfer in metallic powders can be calculated on the basis of the radiation transfer equation where a powder bed is characterised by the following effective parameters: extinction coefficient β, albedo ω, and scattering phase function P. In the geometrical optics approximation, the extinction coefficient is determined by the structure of powder, i.e. by size and shape of particles and by their arrangement, but is independent of optical properties of the material of particles like reflectance. In case of opaque particles, one can estimate extinction coefficient as a quarter of powder surface per unit pore volume. This takes into account dependent scattering that increases the extinction coefficient in inverse proportion to porosity. On the contrary, the scattering characteristics as albedo and phase function depend on reflective properties of the material of particles. For example, albedo is equal to hemispherical reflectance when there is no preferential orientation of particles. Dependent scattering can be neglected when estimating the albedo and the phase function of metallic powders, even at high densities.

The typical configuration of laser treatment of powders is normal incidence of collimated radiation on a thin powder layer deposited on a reflective substrate. The radiation transfer equation for this configuration is analytically solved by the two-flux method. The models of isotropic specular and diffuse reflection are applied. Energy deposition profiles and integral absorptances are calculated for the considered system. The results obtained in the limit of deep powder bed essentially agree with ray tracing simulation [4,8]. Due to multiple reflections in an open pore system, laser radiation can penetrate into the powder to considerable depths, much greater than the characteristic particle diameter. Scattered radiation component formed by multiple reflections in metallic powders becomes more intensive than collimated component originated from the incident laser radiation. Summarising the behaviour of thin powder layers on reflecting substrates, one can say that the total laser energy absorbed in the layer increases with its thickness but the deposited energy density decreases. Generally, absorptance and energy density for the specular reflection model are slightly greater than these values for the diffuse reflection model. This is because backward scattering is more intensive at diffuse reflection.

The obtained theoretical results are in good agreement with experimentally observed correlation between effective absorptance of metallic powders [9] and absorptance of corresponding dense metals.

References

[1] S. Barnes, N. Timms, B. Bryden, I. Pashby, High power diode laser cladding, J. Mater. Process. Technol. 138 (2003) 411–416.

[2] J.-P. Kruth, P. Peeters, T. Smolderen, J. Bonse, T. Laoui, L. Froyen, Comparison between CO_2 and Nd:YAG lasers for use with selective laser sintering of steel-copper powders, Int. J. CAD/CAM Comput. Graphics 13 (1998) 95–110.

[3] C. Over, W. Meiners, K. Wissenbach, J. Hutfless, M. Lindemann, Rapid manufacturing of metal parts and tools using laser melting, in: R. Poprawe, A. Otto (Eds.), Lasers in Manufacturing 2003, AT-Verlag, Stuttgart, 2003, pp. 265–270.

[4] X.C. Wang, J.-P. Kruth, A simulation model for direct selective laser sintering of metal powders, in: B.H.V. Topping (Ed.), Computational Techniques for Materials, Composites and Composite Structures, Civil-Comp, Edinburg, 2000, pp. 57–71.

[5] B.P. Singh, M. Kaviany, Modelling radiative heat transfer in packed beds, Int. J. Heat Mass Transfer 35 (1992) 1397–1405.

[6] D. Baillis, J.F. Sacadura, Thermal radiation properties of dispersed media: theoretical prediction and experimental characterisation, J. Quant. Spectrosc. Radiat. Transfer 67 (2000) 327–363.
[7] R. Siegel, J.R. Howell, Thermal Radiation Heat Transfer, Hemisphere, New York, 1981.
[8] X.C. Wang, T. Laoui, J. Bonse, J.P. Kruth, B. Lauwers, L. Froyen, Direct selective laser sintering of hard metal powders: experimental study and simulation, Int. J. Adv. Manuf. Technol. 19 (2002) 351–357.
[9] N.K. Tolochko, T. Laoui, Yu.V. Khlopkpv, S.E. Mozzharov, V. Titov, M.B. Ignatiev, Absorptance of powder materials suitable for laser sintering, Rapid Prototyping J. 6 (2000) 155–160.
[10] H.C. Van de Hulst, Light Scattering by Small Particles, Dover, New York, 1981.
[11] B.L. Drolen, C.L. Tien, Independent and dependent scattering in packed-sphere system, J. Thermophys. 1 (1987) 63–68.
[12] J.C. Chen, S.W. Churchill, Radiant heat transfer in packed beds, AIChE J. 9 (1963) 35–41.
[13] K. Kamiuto, M. Iwamoto, M. Sato, T. Nishimura, Radiation-extinction coefficients of packed-sphere systems, J. Quant. Spectrosc. Radiat. Transfer 45 (1991) 93–96.
[14] P.D. Jones, D.G. McLeod, D.E. Dorai-Raj, Correlation of measured and computed radiation intensity exiting a packed bed, J. Heat Transfer 118 (1996) 94–102.
[15] K. Kamiuto, Correlated radiative transfer in packed-sphere systems, J. Quant. Spectrosc. Radiat. Transfer 43 (1990) 39–43.
[16] M. Tancrez, J. Taine, Direct identification of absorption and scattering coefficients and phase function of a porous medium by a Monte Carlo technique, Int. J. Heat Mass Transfer 47 (2004) 373–383.
[17] S. Torquato, B. Lu, Chord-length distribution function for two-phase random media, Phys. Rev. E 47 (1993) 2950–2953.
[18] D.E. Gray (Ed.), American Institute of Physics Handbook, McGraw-Hill, New York, 1972.
[19] E.D. Palik (Ed.), Handbook of Optical Constants of Solids, Academic Press, New York, 1985.
[20] E.D. Palik (Ed.), Handbook of Optical Constants of Solids II, Acad. Press, New York, 1991.
[21] M. Bass (Ed.), Handbook of Optics, vol. 2, McGraw-Hill, New York, 1995.
[22] D.R. Lide (Ed.), CRC Handbook of Chemistry and Physics, CRC Press, New York, 2000.